

Valence Bond Concepts Applied to the Molecular Mechanics Description of Molecular Shapes. 2. Applications to Hypervalent Molecules of the P-Block

Thomas Cleveland and Clark R. Landis*

Contribution from the Department of Chemistry, University of Wisconsin, Madison, Wisconsin 53706

Received February 27, 1995. Revised Manuscript Received March 10, 1996[⊗]

Abstract: A fascinating aspect of inorganic chemistry is the occurrence of complicated and varied molecular shapes. However, these same features lead to difficulties in developing molecular mechanics (MM) methods that are suitable for inorganic molecules. In this paper we demonstrate that simple valence bond concepts can guide the construction of a new MM force field for hypervalent molecules of the p-block of the periodic table. The primary difficulty in applying valence bond concepts to the MM description of hypervalent molecular shapes is the occurrence of intrinsically delocalized bonding arrangements, such as the three-center four-electron bond of XeF₂. The inclusion of resonating configurations into the MM method provides a mechanism for surmounting the difficulties presented by hypervalent molecules. By making the contributions of the individual configurations to the total potential energy function dependent on the molecular geometry, we find that both equilibrium geometries and fluxional pathways of hypervalent molecules can be modeled with impressive accuracy. This model, which we call HyperValent Valence Bond (HV-VB), is readily extended to hypervalent molecules containing mixed ligands. By using the valence bond model to derive the HV-VB method, the results of our MM computations indirectly become discriminating tests of the basic concepts of the model. The ideas that Pauling first presented more than six decades ago exhibit remarkable robustness.

I. Introduction

The value of molecular mechanics (MM) computations for exploring the structures and dynamics of organic molecules is established well due to the pioneering efforts of Westheimer,¹ Lifson,² Allinger,^{3–7} and others.⁸ More recently, programs such as CHARMM^{9,10} and AMBER¹¹ have demonstrated the utility of MM computations in biomolecular simulations. A result of these successes is a growing interest in extending the range of molecular mechanics applications to encompass the entire periodic table,^{12–17} thus spanning inorganic as well as organic chemistry. However, as noted by us^{18,14} and by others,^{19–23,15}

the extension of the molecular mechanics method throughout the entire periodic table is fraught with difficulties. Prominent difficulties include (1) describing complex molecular shapes, (2) treating indistinct topologies (i.e., structures for which the location of electron pair bonds is uncertain), and (3) parameterization. These problems are particularly severe for hypervalent main group compounds and transition metal complexes; for such molecules one must deal with high coordination numbers and the attendant multiple equilibrium bond angles, highly delocalized bonding modes for unsaturates (such as the cyclopentadienyl–metal interaction), high bond ionicity, and the prospect of generating thousands of new parameters.

Molecular mechanics may be viewed as a computational expression of simple bonding models. Previously we have shown that consideration of bonding models such as the angular overlap method¹⁴ and valence bond theory (the VALBOND¹⁷ force field) can lead to improved MM descriptions of inorganic and organic structures. In the VALBOND scheme it was shown that the localized bonding concepts of valence bond theory provide a natural basis for MM computations, which are formulated in terms of localized bond topologies. In this paper we present the conceptual viewpoint, the algorithms, and the performance of the VALBOND scheme as extended to hypervalent main group compounds. We refer to this extended version of the force field as HV-VB (HyperValent Valence Bond). We focus on hypervalent molecules in order to (1) directly address some of the contemporary problems in the application of MM across the periodic table and (2) explore

[⊗] Abstract published in *Advance ACS Abstracts*, June 1, 1996.

(1) Westheimer, F. H. *Steric Effects in Organic Chemistry*; John Wiley: New York, 1956.

(2) Lifson, S.; Warshel, A. *J. Chem. Phys.* **1968**, *49*, 5116.

(3) Allinger, N. L.; Sprague, J. *J. Am. Chem. Soc.* **1973**, *95*, 3893.

(4) Allinger, N. L. *J. Am. Chem. Soc.* **1977**, *99*, 8127.

(5) Allinger, N. L.; Yuh, Y. H.; Lii, J.-H. *J. Am. Chem. Soc.* **1989**, *111*, 8551.

(6) Allinger, N. L.; Lii, J.-H. *J. Am. Chem. Soc.* **1989**, *111*, 8566.

(7) Allinger, N. L.; Lii, J.-H. *J. Am. Chem. Soc.* **1989**, *111*, 8576.

(8) Rasmussen, K. *Potential Energy Functions in Conformational Analysis*; Springer-Verlag: Berlin, 1985; Vol. 37, pp 231.

(9) Brooks, B. R.; Bruccoleri, R. E.; Olafson, B. D.; States, D. J.; Swaminathan, S.; Karplus, M. *J. Comput. Chem.* **1983**, *4*, 187.

(10) Brooks, C. L., III; Karplus, M.; Pettitt, B. M. *Proteins: A Theoretical Perspective of Dynamics, Structure, and Thermodynamics*; John Wiley & Sons: New York, 1988; Vol. LXXI.

(11) Weiner, P.; Kollman, P. *J. Comput. Chem.* **1981**, *2*, 287.

(12) Casewit, C. J.; Colwell, K. S.; Rappé, A. K. *J. Am. Chem. Soc.* **1992**, *114*, 10046.

(13) Casewit, C. J.; Colwell, K. S.; Rappé, A. K. *J. Am. Chem. Soc.* **1992**, *114*, 10035.

(14) Allured, V. S.; Kelly, C.; Landis, C. R. *J. Am. Chem. Soc.* **1991**, *113*, 1.

(15) Rappé, A. K.; Casewit, C. J.; Colwell, K. S.; Goddard, W. A. I.; Skiff, W. M. *J. Am. Chem. Soc.* **1992**, *114*, 10024.

(16) Rappé, A. K.; Colwell, K. S.; Casewit, C. J. *Inorg. Chem.* **1993**, *32*, 3438.

(17) Root, D. M.; Landis, C. R.; Cleveland, T. *J. Am. Chem. Soc.* **1993**, *115*, 4201.

(18) Doman, T. N.; Landis, C. R.; Bosnich, B. *J. Am. Chem. Soc.* **1992**, *114*, 7264.

(19) Hay, B. P. *Coord. Chem. Rev.* **1993**, *126*, 177.

(20) Hancock, R. D. *Progress In Inorganic Chemistry* **1989**, *37*, 187.

(21) Gajewski, J. J.; Gilbert, K. E.; McKelvey, J. In *Advances in Molecular Modeling*; D. Liotta, Ed.; JAI Press: Greenwich, CT, 1990; Vol. 2; pp 65.

(22) Comba, P. *Coord. Chem. Rev.* **1993**, *123*, 1.

(23) Vedani, A. *J. Comput. Chem.* **1988**, *9*, 269.

the forces determining molecular shapes in this interesting class of molecules. We consider only molecules that are hypervalent in the σ framework (e.g., XeF₂) and exclude from consideration those molecules which may be considered hypervalent by virtue of the presence of multiple bonds between the central atom and the ligand (e.g., Me₃P=O). There has been much debate over the use of the term hypervalent.^{24–26} We use hypervalent as defined by Musher: atomic centers are hypervalent “which exceed the number of valences allowed by the traditional theory, and thus utilize more electron-bonding pairs than provide stability in the Lewis–Langmuir theory”.²⁷

We begin this paper by briefly reviewing previous MM approaches to modeling hypervalent molecules. This section is followed by a short review of bonding models that have been used to describe hypervalency. The subsequent section presents a concise overview of the features of the nonhypervalent VALBOND scheme which are essential to the development of HV-VB. Our presentation of the HV-VB method begins with a description of the simple hypervalent molecule, XeF₂. Hypervalent molecules that contain more than two ligands require a more complex treatment. Using ClF₃ as an example, we next show that inclusion of resonating configurations into the MM method enables good descriptions of equilibrium geometries, ligand interchange dynamics, and vibrational frequencies of hypervalent molecules containing more than two ligands. The following section presents a simple scheme for treating the site preferences of different ligands for inequivalent coordination sites (e.g., equatorial vs axial PF₄Me). Results obtained from the application of HV-VB to a variety of main group hypervalent compounds are compared with experimental results.

II. Molecular Mechanics Approaches to Hypervalent Molecules

A variety of approaches have been used to describe the shapes, energetics, and dynamics of hypervalent main group molecules. Perhaps the simplest approach is the Points-On-a-Sphere (POS) model.^{19,28–33} In the points on a sphere model, molecular shapes are controlled by 1,3-interactions (or ligand–ligand) interactions. The primary difference between various POS models is the choice of 1,3-interaction potential.

Valence model formulations of MM force fields for the geometries of hypervalent molecules emphasize bonding interactions and their stabilities as a function of geometry. For example, our formulation of the SHAPES force field¹⁴ used periodic trigonometric functions and spherical internal coordinates to describe the angular potential energies in main group and transition metal complexes. The form of the SHAPES energy functions can be rationalized on the basis of maximization of orbital overlaps according to the Angular Overlap Model (AOM). Similar angle terms expressed in the usual internal coordinates have been used by Rappé and co-workers¹⁵ (UFF force field) and by Vedani and co-workers³⁴ (YETI force field). In general, these methods have focused on general descriptions

of idealized molecular shapes. Although these schemes have made molecular mechanics computations possible for inorganic problems, they all presume that the user know the idealized shape of the molecule at the outset. Thus, unlike the POS models, they are not truly predictive. In addition, these approaches may be overly biased to the assumed preferred idealized shape. We have found, for example, that the trigonal bipyramidal geometry representation in the SHAPES force field is too rigid with respect to distortion to the square pyramidal geometry.³⁵

An attractive strategy for making MM force fields more general and more predictive is to reformulate the potential energy expression in terms of a more fundamental bonding theory. Because MM computations are based on localized bond topologies, valence bond theory is a natural choice. Using the simple principles of the directed covalent bond formulated by Pauling^{36,37} more than six decades ago, we have derived new MM bond angle terms. These terms form the basis of the VALBOND force field¹⁷ and exhibit the following properties: faithful representation of bending potential energy surfaces over large angular distortions, prediction of the idealized molecular geometry via the fundamental concepts of hybridization and Lewis structures, and general parametrization via rule-based algorithms based on familiar concepts such as Bent’s rule.³⁸ The VALBOND force field reproduces the structures and vibrational frequencies of nonhypervalent organic and inorganic molecules from the p-block of the periodic table. Rappé and co-workers³⁹ recently have shown that this orbital viewpoint also facilitates the description of bond-making and -breaking process in a MM computation. However, molecules that exceed the capacity of the central atom’s valence orbitals to form two electron bonds to each of the ligands (e.g., hypervalent molecules) and molecules for which hybridization prescriptions are uncertain (e.g., transition metal complexes) cannot be treated with the previous VALBOND scheme. Thus, we have sought to extend the VALBOND scheme to hypervalent molecules.

III. XeF₂: A Simple Hypervalent Molecule

A. Hypervalent Bonding Models. The literature contains many vigorous discussions^{27,40–53} of the nature of hypervalent bonding. Consider XeF₂, the simplest hypervalent molecule (simplest because it has just two ligands and the total number of valence electrons exceeds an octet by just two electrons). Thirty years ago⁴² Coulson reviewed four models of the bonding in XeF₂: (1) d^mspⁿ hybridization, (2) correlation effects model, (3) delocalized molecular orbital model, and (4) valence bond resonance model. In the time since Coulson’s review, several

(24) Schleyer, P. v. R. *Chem. Eng. News* **1984**, 62, 4.
 (25) Martin, J. C. *Chem. Eng. News* **1984**, 62, 4.
 (26) Harcourt, R. D. *Chem. Eng. News* **1985**, 63, 3.
 (27) Musher, J. *Angew. Chem., Int. Ed. Engl.* **1969**, 8, 54.
 (28) Deiters, J. A.; Gallucci, J. C.; Clark, T. E.; Holmes, R. R. *J. Am. Chem. Soc.* **1977**, 99, 5461.
 (29) Holmes, R. R. *Pentacoordinated Phosphorous*; American Chemical Society: Washington, DC, 1980; Vol. 1–2.
 (30) Bartell, L. S.; Plato, V. *J. Am. Chem. Soc.* **1973**, 95, 3097.
 (31) Bartell, L. S. *Croat. Chem. Acta* **1984**, 57, 927.
 (32) Hay, B. P. *Inorg. Chem.* **1990**, 30, 2876.
 (33) Kepert, D. L. *Inorganic Stereochemistry*; Springer-Verlag: Berlin, 1982.
 (34) Vedani, A.; Huhta, D. W. *J. Am. Chem. Soc.* **1990**, 112, 4759.

(35) Root, D. M.; Landis, C. R.; unpublished results.
 (36) Pauling, L. *Proc. Natl. Acad. Sci. U.S.A.* **1928**, 14, 359.
 (37) Pauling, L. *J. Am. Chem. Soc.* **1931**, 58, 1367.
 (38) Bent, H. *Chem. Rev.* **1961**, 61, 275.
 (39) Rappé, A. J.; unpublished results.
 (40) Pimentel, G. C. *J. Chem. Phys.* **1951**, 19, 446.
 (41) Rundle, R. E. *Rec. Chem. Prog.* **1962**, 23, 194.
 (42) Coulson, C. A. *J. Chem. Soc.* **1964**, 1442.
 (43) Coulson, C. A. *J. Chem. Phys.* **1966**, 44, 468.
 (44) Musher, J. L. *J. Am. Chem. Soc.* **1972**, 94, 1370.
 (45) Bagus, P. S.; Liu, B.; Schaefer, H. F. *J. Am. Chem. Soc.* **1972**, 94, 6635.
 (46) Bagus, P. S.; Liu, B.; Liskow, D. H.; Schaefer, H. F. *J. Am. Chem. Soc.* **1975**, 97, 7216.
 (47) Hay, P. J. *J. Am. Chem. Soc.* **1977**, 99, 1003.
 (48) Kiang, T.; Zare, R. N. *J. Am. Chem. Soc.* **1980**, 102, 4024.
 (49) Kutzelnigg, W. *Angew. Chem., Int. Ed. Engl.* **1984**, 23, 272.
 (50) Kutzelnigg, W. *J. Mol. Struct.* **1988**, 169, 403.
 (51) Reed, A. E.; Schleyer, P. v. R. *J. Am. Chem. Soc.* **1990**, 112, 1434.
 (52) Magnusson, E. *J. Am. Chem. Soc.* **1990**, 112, 7940.
 (53) Cooper, D. L.; Cunningham, T. P.; Gerratt, J.; Karadakov, P. B.; Raimondi, M. *J. Am. Chem. Soc.* **1994**, 116, 4414.

noteworthy refinements to the analysis of hypervalent bonding have appeared.^{27,44,46–49,51–54} For example, numerous authors have shown that d-orbitals act as polarization functions, not true participants in hybridization.^{44,47,49,51–54}

The valence bond model emphasizes the resonance among the ionic structures, $F-Xe^+ F^-$ and $F^- +Xe-F$, and the long bond structure, $F \cdot Xe: F \cdot$. Many features of this model parallel those of molecular orbital theory. Most striking are the similarity in charge distributions and, hence, the necessity of electronegative ligands for stabilizing the ionic structures. Resonance results in delocalization of the electron density over all three atoms and an attendant lowering of the total energy. Coulson showed that the molecular orbital determinantal wave function can be recast in terms of resonating valence bond structures. The molecular orbital model emphasizes more ionic terms (such as $F^- Xe^{2+} F^-$) than the two resonance configuration valence bond model. A disadvantage of the valence bond model is a general ignorance of the signs and magnitudes of the various matrix elements involving the resonating configurations. Thus, the angular dependence of the resonance interaction is not obvious. Qualitatively, one suspects that the $+Xe-F$ electron pair bond has largely Xe p-character, thus suggesting maximum resonance stabilization at the linear geometry.

B. The VALBOND MM Scheme. The VALBOND treatment of angular potentials is based on minimizing the overlap of bonding hybrid orbitals.¹⁷ Given that two bond orbitals have a preferred hybridization, the overlaps and the orbital strengths (i.e., the angular parts of the hybrid wave functions) of these two orbitals at any bond angle can be computed readily (1–3). A non-zero overlap leads to a decrease in the hybrid orbital strengths; the change in strengths from their maximum values for a given hybridization is termed a pair defect. In the VALBOND scheme, the energy penalty is linearly proportional to the magnitude of the pair defect (4). For molecules with more than two bonds to a central atom, summation of the pair defect energies for all bond pairs yields the angular energy about that central atom. VALBOND uses simple constructs such as Lewis dot structures and Bent's rule to estimate the preferred hybridizations of each bond in a molecule. We previously have

$$S(\alpha) = S^{\max} \sqrt{1 - \frac{1 - \sqrt{(1 - \Delta^2)}}{2}} \quad (1)$$

where the nonorthogonality integral, Δ , at the interhybrid orbital angle, α , for two hybrids with $sp^m d^n$ hybridization is given by

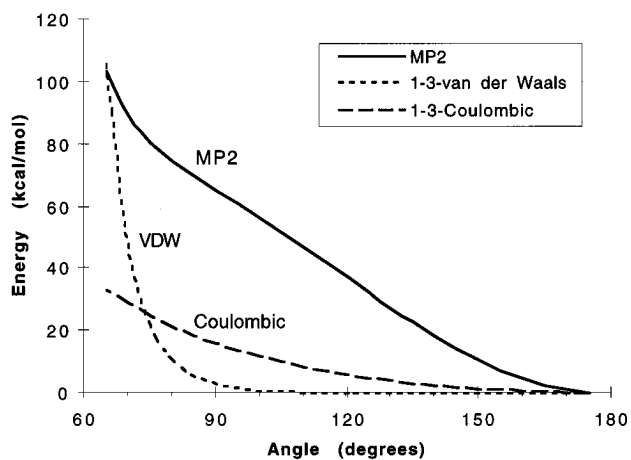
$$\Delta = \frac{1}{1 + m + n} \left(1s + m \cos \alpha p_z + \frac{n}{2} (3 \cos^2 \alpha - 1) dz^2 \right) \quad (2)$$

$$S^{\max} = \sqrt{\frac{1}{1 + m + n}} (1 + \sqrt{3m} + \sqrt{5n}) \quad (3)$$

$$E(\alpha) = \sum_{\text{all L-M-L angles}(\alpha)} k(S^{\max} - S(\alpha)) \quad (4)$$

demonstrated that VALBOND¹⁷ accurately reproduces the geometries, vibrational frequencies, and the shape of the potential energy surfaces for nonhypervalent molecules from the p-block of the periodic table.

C. Angular Dependence of the Three-Center, Four-Electron ($3c-4e^-$) Bond. In extending the VALBOND scheme



(a)

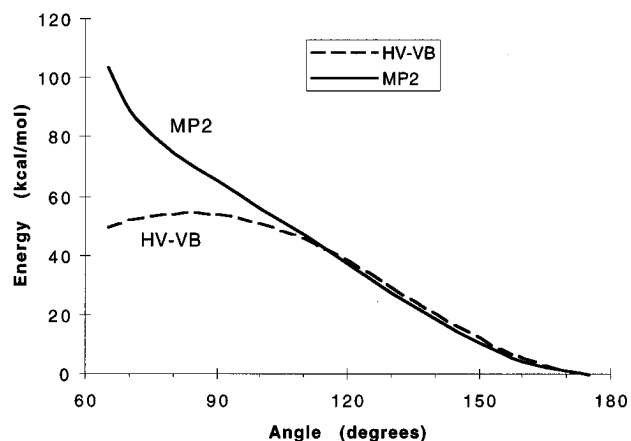


Figure 1. (a) Plots of the ab initio (MP2/LANL1DZ), Coulombic, and van der Waals energies as a function of the bond angle in XeF_2 . (b) Plots of the ab initio (MP2) and the HV-VB energies as a function of bond angle.

to hypervalent molecules we seek to retain the localized, hybrid orbital viewpoint. Furthermore, we require that the model be consistent with the results of modern electronic structure computations; e.g., d-orbitals are not used in the hybridization of XeF_2 . Finally, the method should lend itself to generic, rule-based parametrization and give accurate structures, dynamic behavior, and vibrational frequencies.

A natural starting point is to describe XeF_2 bonding as the resonance of two valence bond structures: $F-Xe^+ F^-$ and $F^- +Xe-F$. From here on we denote the $3c-4e^-$ bond resonance with the single diagram, $F \cdots Xe \cdots F$. N.B., in our scheme, the $3c-4e^-$ bond actually represents an equal mixture of two resonance structures; each resonance structure has one $2c-2e^-$ covalent bond and one F^- . Thus, the net covalent bond order for each Xe and F interaction is approximately 1/2. The charge distribution of XeF_2 as well as the dependence of the molecular stability on the presence of two electronegative ligands and a central atom with a low ionization potential follow from this resonance prescription. However, these simple configurations do not suggest how the molecular energy will change as a function of bond angle. Computations of the angular potential energy of XeF_2 as a function of bond angle at the MP2 level are shown in Figure 1a. Also shown are the energies arising from F–F van der Waals interactions and Coulombic interactions based on the CHARMM⁹ functional forms and parameters. Clearly, the angular potential energy surface is not described well by 1,3-Coulombic or a 1,3-van der Waals interactions,

Table 1. Comparison of Electron Density in Localized NBOs for Hypervalent and Nonhypervalent Molecules

molecule	% electron density in localized orbitals
CH ₄	99.98
NH ₃	99.99
H ₂ O	99.99
PCl ₅	99.113
ClF ₃	99.145
XeF ₂	99.54
XeF ₂ (NRT)	99.95

either alone or in combination. Thus, if one adopts the common MM convention of not explicitly including lone pairs in the computation, one must include terms that account for the influence of orbital interactions on the angular potential energy surface.

The Natural Bond Orbital (NBO)^{55–58} and Natural Resonance Theory (NRT) methods⁵⁹ developed by Weinhold and co-workers are powerful tools for extracting localized bonding descriptions from high level electronic structure computations. The ultimate validity of the VALBOND approach requires that localized, hybrid bond orbitals accurately describe the electron density distributions in molecules. Therefore, we have carried out extensive NBO and NRT analyses of simple hypervalent molecules.⁶⁰ For computations involving elements past chlorine, LANL1DZ⁶¹ was used; all electron computations using the 6-311G** basis set were used for the lighter elements. For nonhypervalent molecules, Weinhold and co-workers⁵⁵ have shown that localized NBOs commonly account for >99.98% of the total electron density distribution. Furthermore, these NBOs have hybridizations that commonly involve little bond bending, are transferable among similar molecules, and follow the patterns of Bent's rule. In contrast localized bond models based on just one Lewis structure for XeF₂ and other hypervalent molecules give relatively poor descriptions of the electron density distribution (Table 1). For example, the F[−] +Xe−F Lewis structure accounts for just 99.5% of the total electron density distribution of XeF₂. The problem here lies with the lack of resonance with the F−Xe⁺F[−] structure. Indeed, analysis of the electron density by NRT with two Lewis structures in resonance accounts for 99.95% of the total electron density.

Even at the level of single configuration analysis, the NBO model provides a rationalization for the dependence of the XeF₂ energy on bond angle. In addition to one Xe−F polar covalent bond, the NBOs of XeF₂ exhibit a strong delocalization of one of the F[−] lone pairs (lp) into the Xe−F antibond (σ^*). This stabilizing donor–acceptor interaction is essentially that which Weinhold and others have used to describe intermolecular hydrogen bonding interactions.⁵⁸ Given the analogy between FHF[−] and FXeF first suggested by Pimentel,⁴⁰ it is not surprising

(55) Reed, A. E.; Weinhold, F.; Curtiss, L. A.; Pochatko, D. J. *J. Chem. Phys.* **1986**, *84*, 5687.

(56) Carpenter, J. E.; Weinhold, F. *J. Am. Chem. Soc.* **1988**, *110*, 368.

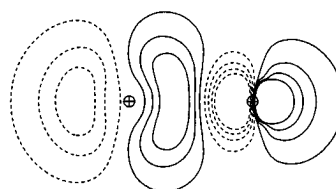
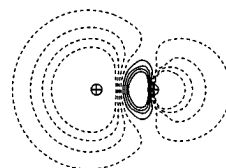
(57) Foster, J. P.; Weinhold, F. *J. Am. Chem. Soc.* **1980**, *102*, 7211.

(58) Reed, A. E.; Curtiss, L. A.; Weinhold, F. *Chem. Rev.* **1988**, *88*, 899.

(59) Glendening, E. D.; Weinhold, F. "Natural Resonance Theory. I. General Formalism," University of Wisconsin Theoretical Chemistry Institute, 1994.

(60) Frisch, M. J.; Trucks, G. W.; Head-Gordon, M.; Gill, P. M. W.; Wong, M. W.; Foresman, J. B.; Johnson, B. G.; Schlegel, H. B.; Robb, M. A.; Replege, E. S.; Gomperts, R.; Andres, J. L.; Raghavachari, K.; Binkley, J. S.; Gonzales, C.; Martin, R. L.; Fox, D. J.; Defrees, D. J.; Baker, J.; Stewart, J. J. P.; Pople, J. A. *Gaussian 92*, Revision E.2; Gaussian, Inc.: 1992.

(61) LANL1DZ represents a computation using an effective core potential for all but the valence electrons which were explicitly represented with a double- ζ basis set, as described in Wadt, W. R.; Hay, P. J. *J. Chem. Phys.* **1985**, *82*, 284.

+Xe-F Antibond Orbital**H-F Antibond Orbital****Figure 2.** Electron density plots of the antibonding orbitals of ⁺Xe−F and H−F.**Table 2.** Computed Vibrational Frequencies of XeF₂

mode	HV-VB ($k = 220$)	ab initio ^a	experiment ^b
π_u	197	227	213
σ_g^+	511	543	515
σ_g^-	580	554	558

^a HF/6-311G**. ^b Jones, L. *Inorganic Vibrational Spectroscopy*; Marcel Dekker: New York, 1971; Vol. 1, p 59.

that NBO analysis of XeF₂ leads to a picture that it is remarkably similar to that of the bifluoride ion (Figure 2). One expects that the stabilization afforded by the lp $\rightarrow \sigma^*$ donor–acceptor interaction will depend on the overlap of the interacting orbitals.⁶² Thus, the hybridization of the ⁺Xe−F σ^* orbital largely determines the shape of the bending potential. Because the ⁺Xe−F σ^* has a Xe hybrid component which is essentially a 180° phase-shifted ⁺Xe−F σ -bonding hybrid, we suggest the following form of the potential energy expression

$$E(\alpha) = \text{BOF} \times k_\alpha [1 - \Delta(\alpha + \pi)^2] \quad (5)$$

where α is the bond angle, k_α is the VALBOND parameter, BOF is a bond order factor (equal to 0.25 in this example), and Δ is the overlap integral.

The essence of this expression is that the energy of the 3c−4e[−] interaction is proportional to the square of the overlap between the ⁺Xe−F σ^* hybrid orbital and a F[−] lone pair. The BOF has a value of 0.25 for a 3c−4e[−] term and is described in detail for the example of ClF₃ (vide infra). A graph of the potential energy surface for XeF₂ using this function with sp¹⁰ hybridization is shown in Figure 1b. Clearly, the shape of the MP2 ab initio surface arises principally from the orbital interactions. The electrostatic and van der Waals terms mainly influence the shape at bond angles less than 90°. Thus, we conclude that orbital interactions determine the shape of the potential energy curve at large bond angles, and 1,3-interactions dominate at very small bond angles. Note that these explanations neglect any direct influence of lone pairs.

Vibrational frequencies sensitively test the curvature of the bending potential energy surface. As shown in Table 2, the experimental vibrational frequencies of XeF₂⁶³ are modeled reasonably well for a purely diagonal force field. In these, and

(62) Landis, C. R. In *Advances in Molecular Structures*; Hargittai, I. Hargittai, M., Eds.; JAI Press: Greenwich, CT, 1996; Vol. 2, pp 129–161.

(63) Nakamoto, K. *Infrared and Raman Spectra of Inorganic and Coordination Compounds*, 4th ed.; Wiley: New York, 1986.

all other computations using the HV-VB force field presented here, the generic VALBOND scaling parameter of $k_a = 220$ kcal/mol is used. The standard CHARMM force field terms and parameters were used for bond stretch, proper dihedrals, improper dihedrals, and van der Waals terms.⁹ Electrostatics were not used in these calculations.

IV. ClF₃: Contributions from both 2c–2e[–] and 3c–4e[–] Bonds

The “excess” electrons in hypervalent molecules are accommodated in 3c–4e[–] bonds. Each pair of electrons in excess of eight electrons requires the presence of one 3c–4e[–] bonding unit. Thus by our partitioning scheme, ClF₃ has one 3c–4e[–] bonding interaction, one 2c–2e[–] bond, and two lone pairs. Because the 3c–4e[–] bonding unit prefers a linear arrangement of ligands and because the Cl–F 2c–2e[–] covalent bond prefers high Cl p-character (or 90° bond angles), one predicts a T-shaped geometry. Related examples having ten valence electrons are XeF₂ (one 3c–4e[–] bond and three lone pairs), SF₄ (one 3c–4e[–] bond, two 2c–2e[–] bonds, and one lone pair), and PF₅ (one 3c–4e[–] bond and three 2c–2e[–] bonds).

A. Generation of Multiple MM Configurations. Molecules that, by our electron counting schemes, contain mixtures of 2c–2e[–] bonds and 3c–4e[–] bonds require a means of designating which atoms are involved in the two types of bond. For a single static structure the primary configuration has the most linear bond pairs designated as the 3c–4e[–] bonds. In order to correctly model large distortions from equilibrium positions (e.g., dynamics of axial-equatorial interchange), one must consider contributions from all possible configurations. The algorithm must generate all configurations, estimate the contributions from the configurations at any given geometry, and smoothly switch among configurations.

Consider the three bonding representations of ClF₃ shown below. We will refer to these as MM configurations; these configurations differ only in the location of the 3c–4e[–] bonding interaction. In a MM computation on structure **A**, we designate angle θ_1 as the hypervalent angle; i.e., θ_1 contains the atoms involved in the 3c–4e[–] interaction. For structure **B** the hypervalent angle is θ_3 , and for structure **C** it is angle θ_2 . Recall that each 3c–4e[–] bond is in fact a resonance of two mixed ionic-covalent Lewis structures.

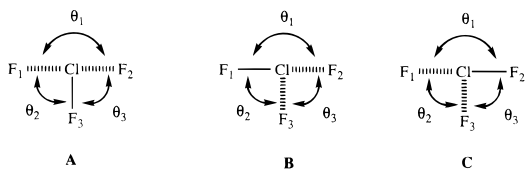


Figure 3. HV-VB weighting coefficients of the three MM configurations (**A**, **B**, and **C**) at four different molecular geometries (**I–IV**).

square of the cosine of the hypervalent angle (θ). Examples of mixing coefficients for four different geometries (**I–IV**) of ClF₃

$$c_j = \frac{\prod_{i=1}^{\text{hype}} \cos^2 \theta_i}{\sum_{j=1}^{\text{config}} \prod_{i=1}^{\text{hype}} \cos^2 \theta_i} \quad (7)$$

(where config = number of resonance configurations and hype = number of hypervalent angles)

are shown in Figure 3. In this figure, the geometries **I**, **III**, and **IV** correspond to the three redundant T-shapes that are distinguished only by atom labeling.

The angle terms in HV-VB are scaled by a bond order factor (BOF). This is best explained by example. Consider the MM configuration **A** for ClF₃; the potential energy expression for this MM configuration is given in (8). There are three angular potential energy terms corresponding to the three angles θ_1 – θ_3 . The formal covalent bond orders for the Cl–F₁ and Cl–F₂ bonds are both 1/2 (i.e., a 3c–4e[–] interaction) whereas the Cl–F₃ formal bond order is 1.

$$E_A = 0.25 \times k[1 - \Delta(\theta_1 + \pi)^2] + 0.5 \times [k(S^{\text{max}} - S(\theta_2)) + k(S^{\text{max}} - S(\theta_3))] \quad (8)$$

The challenge is to create a general MM method that is capable of describing the energies of any arbitrary geometry of ClF₃ by appropriate mixing of the MM configurations **A**, **B**, and **C**. This can be accomplished by partitioning the potential energy into a sum of three terms (6). The mixing coefficients (c_A , etc.)

$$E_{\text{tot}} = c_A \times E_A + c_B \times E_B + c_C \times E_C \quad (6)$$

should depend on the molecular geometry and reach limiting values of, e.g., $c_A = 1.0$ and $c_B = c_C = 0.0$ when $\theta_1 = 180^\circ$ and $\theta_2 = \theta_3 = 90.0^\circ$. One function that is consistent with these requirements scales the mixing coefficient according to the

The angle terms for angles θ_2 and θ_3 each involve the interaction of ligands having 1/2 bond order seeking to avoid overlap with a ligand that has a bond order of 1. Thus for these angles the HV-VB term of eq 4 is pre-multiplied by a BOF term of $1 \times 1/2 = 0.5$. By this reasoning the angle term for angle θ_1 is multiplied by BOF = $1/2 \times 1/2 = 0.25$ and the 3c–4e[–] potential energy term of eq 5 is used. For hypervalent molecules with more ligands other combinations arise. For SF₆ (two 3c–4e[–] bonds and two 2c–2e[–] bonds) angle terms involving two ligands both joined by 2c–2e[–] bonds have a BOF = $1 \times 1 = 1$ which pre-multiplies eq 4. Another type of angle term will involve

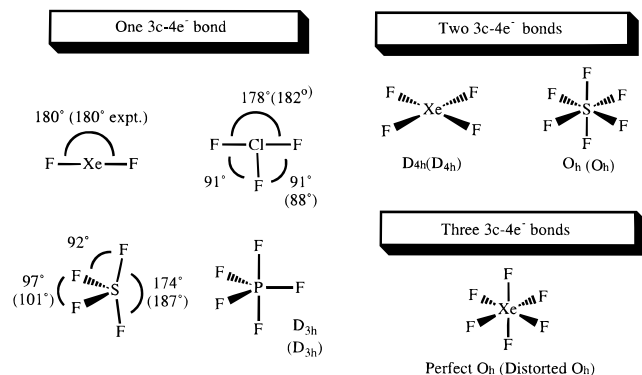


Figure 4. Calculated and experimental shapes for several hypervalent molecules. Experimental geometries are shown in parentheses.

Table 3. Vibrational Frequencies (cm^{-1}) for ClF_3 In-Plane and Out-of-Plane Bending Modes

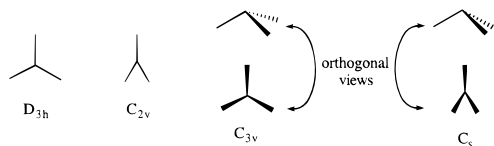
mode	VALBOND	ab initio ^a	experimental ^b
δ (B_2)	418	377	431
π (B_1)	401	431	332
δ (A_1)	328	343	328

^a HF/6-311G**; ^b Frey, R. A.; Redington, R. L.; Aljibury, A. L. K. *J. Chem. Phys.* **1971**, *54*, 344.

two ligands each having bond orders of 1/2 but belonging to two different $3c-4e^-$ bonding interactions. In this case, $\text{BOF} = 1/2 \times 1/2 = 0.25$ but eq 4 is used because the ligands interact to avoid overlap.

B. Results for ClF_3 . The equilibrium geometry generated from this treatment is shown in Figure 4. The default VALBOND parameter of 220 kcal/mol and Cl-F hybridizations of sp^{10} were used in these computations. The bond angles match within 3° of the experimental structure⁶⁴ but are distorted from the ideal T-shape toward the Y-shape rather than toward the arrowhead geometry as is observed experimentally. The vibrational frequencies of ClF_3 bending motions taken from HV-VB computation, HF/6-311G** computation, and experiment⁶⁵ are shown in Table 3. It is seen that the HV-VB geometries and vibrational frequencies agree well with experiment considering the simple form of the purely diagonal force field.

For ClF_3 interesting questions concerning the pathways and transition state barrier heights for the pseudo equatorial-axial exchange process arise. The exchange path could pass through at least four different molecular geometries. (In principle, a variety of asymmetric transition states are possible. However, all pathways must pass through a geometry that contains a symmetry operation that interconverts the originally equatorial F with at least one of the originally axial Fs.) The four that we consider are two planar geometries, the trigonal planar (D_{3h}) and Y-shaped (C_{2v}) geometries, and two nonplanar geometries, the trigonal pyramidal (C_{3v}) and the bent Y-shape (C_s). We know of no simple model that permits prediction of the fluxional pathway.



To our knowledge no experimental measurements of an intramolecular fluxional process for ClF_3 have been reported.

(64) Gillespie, R. J.; Hargittai, I. *The VSEPR Model of Molecular Geometry*; Allyn and Bacon: Boston, 1991.

(65) Frey, R. A.; Redington, R. L.; Aljibury, A. L. K. *J. Chem. Phys.* **1971**, *54*, 344.

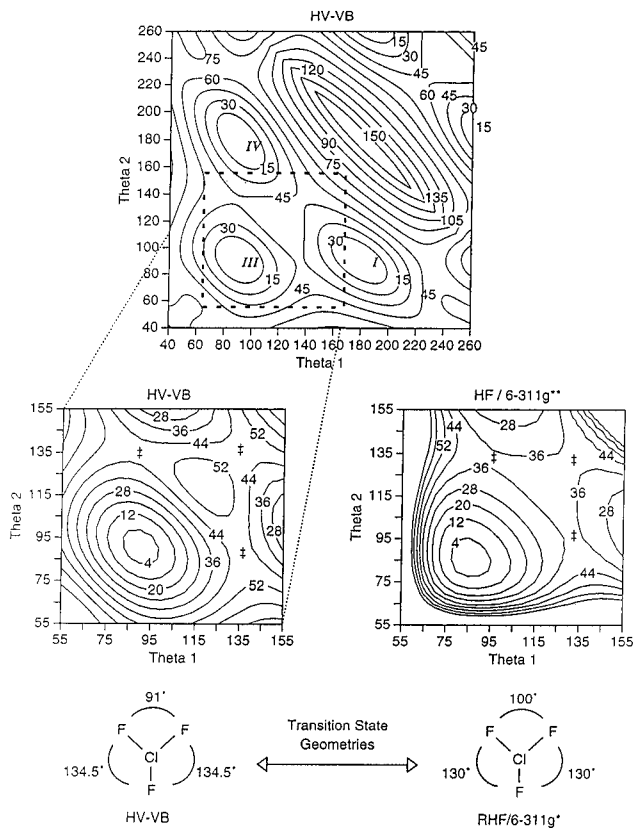


Figure 5. Contour plots of the HV-VB and HF/6-311G** computed potential energy surfaces for angular distortions of ClF_3 . The transition states between the minima are labeled on the plots with a ‡. The italicized roman numerals on the first contour plot represent the geometries from Figure 3; the angle definitions are given in the structural representations of **A**, **B**, and **C**.

Apparently an intermolecular process is sufficiently rapid that measurement of the intramolecular exchange rate is precluded.⁶⁵ Musher²⁷ has considered the magnitude of the exchange barrier and suggested that it should be high because the linearity of the $3c-4e^-$ bonding interaction must be destroyed in any intramolecular exchange pathway. A superficial VSEPR-based analogy between ClF_3 and PF_5 might suggest that a low energy (ca. 5 kcal/mol) Berry pseudorotation process should be possible. However, such a simple one-step process cannot lead to axial-equatorial exchange as the two axial Fs remain equivalent and distinct from the originally equatorial F in the two different square pyramidal intermediates resulting from pseudorotation. Thus at least two pseudorotations are required to effect axial-equatorial exchange. We have used the HV-VB method and ab initio computations to probe the intramolecular exchange pathway.

A comparison of the potential energy surface for planar distortions generated from the HV-VB method and by ab initio (HF/6-311G**) methods is shown in Figure 5. Both surfaces are smooth and free of discontinuities. Each surface has three true minima that correspond to the three redundant T-shaped geometries. Furthermore, both surfaces show true transition states (one imaginary frequency) of C_{2v} geometry along the pathways connecting the minima. A stationary state is found at the D_{3h} geometry; however, it has two imaginary frequencies and is higher in energy than the true C_{2v} transition state. The geometries of the transition state calculated by HV-VB and ab initio methods are shown in Figure 5. The barrier heights for passage from one well to another is 37 kcal/mol from the ab initio surface as compared to 45.8 kcal/mol from the HV-VB surface. The agreement is remarkably good considering the HV-

VB computations use a single default value for the HV-VB parameter (k) without adjustment to achieve a better fit. The smooth, discontinuity free HV-VB surface effects well behaved high temperature dynamics in which the T-shape molecule is observed to undergo numerous axial–equatorial exchanges. Thus, the challenge of multiple equilibrium angle values, that is so problematic on MM simulations of many inorganic compounds, is surmounted satisfactorily, at least for ClF_3 . These results provide a compelling demonstration that our MM scheme can provide a good approximation to the true angular potential energy surface.

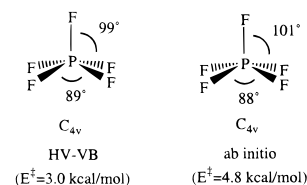
The strong connection of the HV-VB scheme to simple localized bonding concepts permits a simple interpretation of the axial–equatorial exchange process. Preferred fluxional pathways of hypervalent molecules are those that (1) minimize nonorthogonalities of the $2c-2e^-$ bonds with the other ligands and (2) maximize linearity of the $3c-4e^-$ bond interaction. Both of these requirements strongly disfavor nonplanar intermediates (C_s and C_{3v}). The distinction between the D_{3h} and C_{2v} transition states arises from the lower covalent bond orders in the $3c-4e^-$ bonding interaction. In other words, violating the linearity of the $3c-4e^-$ bonding interaction has a smaller energy penalty than nonorthogonalities involving the $2c-2e^-$ bonding interaction. We note that none of this discussion requires consideration of the Cl lone pairs, other than the implicit roles discussed above. Here the preference of ClF_3 for a T-shape equilibrium geometry as well as a C_{2v} geometry for the axial–equatorial exchange is understood on the basis of the directional preferences of the bonding interactions between the central atom and ligands. Thus, the emphasis is quite different from VSEPR ideas in which lone pair repulsions are considered to be as important as the bonds in controlling geometries.

C. Results for Other Homoleptic Hypervalent Compounds. Minimized geometries for a variety of simple hypervalent molecules computed with the hypervalent HV-VB method are shown in Figure 4. Shown with the geometries are the number of MM configurations and the number and types of bonding arrangements. The bonding of SF_4 can be described as two $2c-2e^-$ bonds, one $3c-4e^-$ bond, and one lone pair. In keeping with this arrangement we expect one linear bond angle and the remainder near 90° or the seesaw geometry (C_{2v}). A total of six MM configurations are generated for this structure. Increasing the number of Fs by two to give SF_6 gives two $3c-4e^-$ bonds and two $2c-2e^-$ bonds. This case requires 45 MM configurations, and the computations are correspondingly slower. Although the number of MM configurations is quite large, many of the CPU intensive computations can be streamlined through judicious programming.

All molecular shapes in Figure 4 approximate those found experimentally.⁶⁴ In all cases, the structures are free to exchange inequivalent ligand positions as they move among redundant geometries. However, inspection of the MM geometries of hypervalent molecules reveals a systematic error. The experimental geometries of the hypervalent fluorides exhibit small but consistent distortions of the “linear” bond angles from 180° in a direction that decreases all 1,3 distances. Thus, ClF_3 is bent from the idealized T-shape to the arrowhead geometry by ca. 2° , BrF_5 is distorted from a monovacant octahedron to an umbrella geometry via a 2° distortion, and the axial bond angle of SF_4 is decreased by 3° . In contrast the HV-VB structures exhibit distortions of similar magnitudes *but in the opposite directions*. Thus ClF_3 is distorted slightly toward a Y-shape rather than the arrowhead geometry.

In order to assess better the HV-VB angular potential energy surfaces for hypervalent molecules, we have examined the

axial–equatorial exchange pathway in PF_5 . In agreement with other theoretical studies, we find that the pathway corresponds to the Berry pseudorotation process⁶⁶ using the transition state searching algorithm within CHARMM.⁹ Significantly, we find that the geometries and energies of the transition state for axial–equatorial interconversion essentially are identical for the HV-VB and ab initio computations^{29,67} (see below). The contrast of the barrier heights for axial–equatorial exchange between ClF_3 (ca. 40 kcal/mol)



and PF_5 (ca. 5 kcal/mol) is dramatic. Two effects are operative. First, ClF_3 cannot exchange ligands by a single pseudorotation simply due to the different arrangements of ligands at the equilibrium geometry. If one considers ClF_3 to be a trigonal bipyramid of valence electron pairs, then pseudo-rotation about an equatorial lone pair leads to a high energy, nonplanar structure. Alternatively, pseudo-rotation about the equatorial F maintains the trans disposition of the axial Fs and does not effect axial–equatorial interchange. Second, according to the HV-VB scheme, PF_5 is strained in the trigonal bipyramidal equilibrium geometry, whereas ClF_3 is relatively unstrained. Whereas the T-shape of ClF_3 accommodates the 90° and 180° bond angles preferred by the high p-character $2c-2e^-$ bond and a $3c-4e^-$ bond, respectively, for PF_5 there is no arrangement of five ligands that strainlessly accommodates the preferences of three $2c-2e^-$ bonds for ca. 90° bond angles and a linear $3c-4e^-$ bond. Although the trigonal bipyramid best accommodates the angle preferences of PF_5 , distortion to the C_{4v} geometry involves just a small amount of additional strain.

V. Mixed Ligands and Site Preferences

Hypervalent molecules that contain mixed ligands present complications in MM computations due to the inequivalent isomers generated by the ligands in inequivalent sites.^{29,67} For example, the approximately trigonal bipyramidal PHF_4 may have the H in either equatorial or axial positions. The equatorial isomer is computed to be significantly more stable than the axial isomer. This result agrees with the general observation that the ligand with highest electronegativity prefers an axial site.⁶⁸

A. Basis for Differentiation. The preference of electronegative ligands for axial sites derives from the ionic character and the tendency for linearity of the $3c-4e^-$ bond interaction. The $3c-4e^-$ electron bonding interactions for site isomers of ClF_2H comprise the resonance-stabilized mixture of the ionic structures shown in Figure 6. Clearly the relative isomer stabilities should be proportional to the abilities of the ligands to stabilize negative charge; thus we anticipate that the site preferences should correlate with atomic properties such as electron affinity or electronegativity. Regardless of the particular property chosen, the isomer with both F's in pseudo-axial positions should be favored strongly.

B. Algorithm for Site Preferences and Results. A simple method of incorporating the differential electronic stabilization of site isomers is to offset the MM potential energies of different MM configurations according to atomic properties such as

(66) Berry, R. S. *J. Chem. Phys.* **1960**, *32*, 933.

(67) Strich, A.; Veillard, A. *J. Am. Chem. Soc.* **1973**, *95*, 5574.

(68) Muettterties, E. L. *Acc. Chem. Res.* **1970**, *3*, 266.

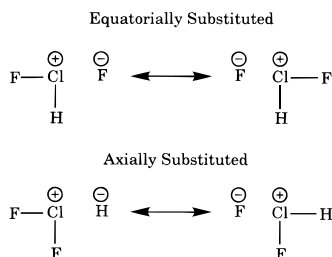


Figure 6. Resonance structures for site isomers of ClF_2H .

Table 4. Relative Site Preference Energies ($E_{R\text{-axial}} - E_{R\text{-equatorial}}$, kcal/mol) for AF_nR Derivatives

molecule	computational method	site preference energy (kcal/mol)
ClF_2H	HV-VB	41.5
	MP2/6-311G**	41.9
ClF_2CH_3	HV-VB	29.2
	MP2/6-311G**	43.3
ClF_2SiH_3	HV-VB	50.3
	MP2/6-311G**	45.3
PF_4H	HV-VB	4.0
	MP2/6-311G**	5.5

electron affinities or electronegativities. Thus, for ClF_2H the MM configuration with H engaged in a three-center, four-electron bond would be offset to higher energy than that with H engaged in a two-center, two-electron bond. We have developed a simple algorithm for offsetting the energies of MM configurations which is based on electronegativities as shown in (9 and 10). The total offset energy, E_{offset} , is a summation over all possible MM configurations for that molecular geometry. The quantity summed is the weighted average of the scaled electronegativities, EN, for the ligands involved in the $3c-4e^-$ bonds in that MM configuration; the weighting factor is the coefficient, c_i , as defined in (7) of the MM configuration.

$$E_{\text{offset}} = \sum_{i=1}^{\text{config}} c_i \sum_{j=1}^{\text{hype}} \frac{\text{EN}_{ija} + \text{EN}_{ijb}}{2} \quad (9)$$

config = number of MM configurations of the site isomer; hype = number of hypervalent angles; a and b refer to the two different atoms of hypervalent angle j in the i th MM configuration; the EN terms are defined below

$$\text{EN}_{ija} = 30 \times (\text{en}_{\text{lig}} - \text{en}_{\text{c.a.}}) \times \text{ss} \quad (10)$$

en_{lig} = electronegativity of ligand; $\text{en}_{\text{c.a.}}$ = electronegativity of central atom; and ss is a scaling factor that is dependent on the sign of the electronegativity difference; the value of ss is 1 if the difference is positive and the value is 2 if it is negative.

The critical attributes of these algorithms are that offset energies are lowest for geometries that have the highest electronegativity ligands (relative to the central atom electronegativity) engaged in linear, $3c-4e^-$ interactions. Conversely, the highest offset energies occur when the ligands engaged in linear, $3c-4e^-$ bonding interactions are less electronegative than the central atom. Although somewhat arbitrary, this algorithm does permit ligand site preferences to be accommodated in a form that is compatible with MM computations and simple bonding models.

The accuracy of the site preference energies has been tested on the mono-substituted homoleptic compounds shown in Table 4. Both the HV-VB and the MP2/6-311G** energies represent differences for fully optimized structures. Given that the MP2 site preference energies do not necessarily represent fully

converged correlation energy corrections, the HV-VB algorithms appear adequate for most purposes.

VI. General Application to Hypervalent Molecules

A demanding test of the HV-VB algorithms and the bonding models that they represent is to apply the method to a wide variety of hypervalent main group molecules. Some comparisons of the HV-VB calculated structures with experimental structures are shown in Table 5. These structures comprise both three- and five-coordinate structures, ligands of varying electronegativity, and both chelating and nonchelating ligand types. Overall the HV-VB computed structures agree well with those determined experimentally, although two notable exceptions are found.

Let us first consider the five-coordinate complexes. Many of the trial compounds contain chelating ligands; the constraints imposed by some chelates can force the normally less stable square pyramidal structure to be preferred.^{29,69} For example, bis(catecholato)methylsilane (**3**), bis(catecholato)adamantylphosphorane (**4**), and bis(catecholato)methylphosphorane (**5**) each are observed to adopt square pyramidal geometries. In each of these compounds the HV-VB minimized structure is a square pyramid with geometries close to the crystallographic values.

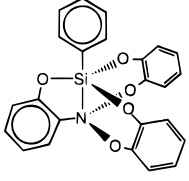
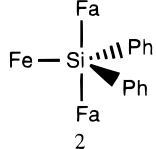
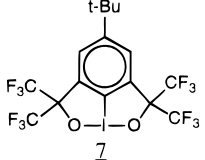
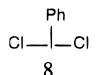
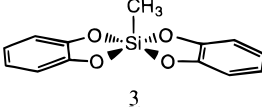
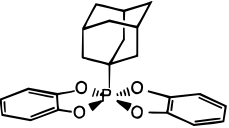
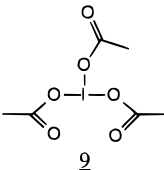
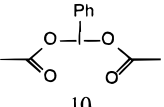
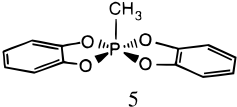
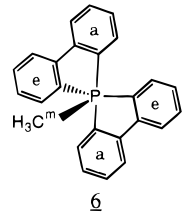
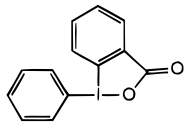
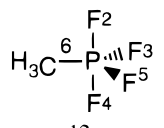
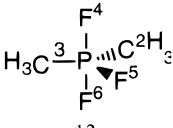
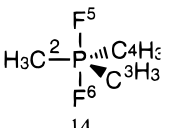
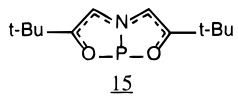
Two problematic five-coordinate structures are phenyl(2,2',2''-nitrotriphenoxy)silane (**1**) and bis(2,2'-biphenylene)methylphosphorane (**6**). For **1**, the discrepancy involves the equatorial O-Si-O bond angles, whereas the crystallographic structure exhibits nearly equivalent bond angles, hence approximate C_3 symmetry, the HV-VB structure shows significant inequivalence among these three angles. The calculated geometry is strongly influenced by the site preference energy offsets. The least electronegative atom (the carbon of the phenyl ring) is in a position that is normally occupied by the most electronegative group. This gives rise to a destabilization of the MM configuration with the phenyl group in the axial position. One might argue that an arene ring group electronegativity might better reflect the ability of the arene ring to stabilize negative charge. Although use of the phenyl group electronegativity⁷⁰ in place of the atomic carbon value improves the fit, the improvement is marginal (two degrees in bond angles). We have found that increasing the phenyl group electronegativity to a value approximately equal to that of oxygen enables the crystallographic structure to be reproduced. Similarly, the deviation of the HV-VB computed geometry (square pyramidal) for **6** from the crystallographic geometry (trigonal bipyramidal) may arise from an enhanced preference of the arene carbons for axial sites, combined with the effects of a small bite angle. Thus the resolution of these discrepancies may lie in the calculation of the site preference energy offset correction by a different method. However, due to the small energy differences (<5 kcal/mol) between most trigonal bipyramids and square pyramids and due to the presence of influences such as crystal packing forces on experimental geometries, it is difficult to assess the origin and significance of the discrepancies between HV-VB and experiment.

A previously noted shortcoming of the HV-VB method is found in the three coordinate iodine compounds. As with ClF_3 , the calculated structures show a preference to distort from a T-shape toward a Y-shape. Experimentally the arrowhead geometry is observed. There are two molecules (10-*tert*-butyl-3,3,7,7-tetrakis(trifluoromethyl)-4,5,6-benzo-1-iodo-2,8-dioxo-

(69) Holmes, R. R.; Day, R. O.; Deiters, J. A.; Swamy, K. C.; Holmes, J. M.; Hans, J.; Burton, S. D.; Prakasha, T. K. In *Developments in Phosphorous Chemistry* American Chemical Society: Washington, DC, 1992; Vol. 486, p 18.

(70) Boyd, R. J.; Boyd, S. L. *J. Am. Chem. Soc.* **1992**, *114*, 1652.

Table 5. Calculated and Experimental Geometries of Some Hypervalent Molecules

 <p style="text-align: center;">1</p>			 <p style="text-align: center;">2</p>			 <p style="text-align: center;">7</p>			 <p style="text-align: center;">8</p>		
PNPOS ^{a,b}	HV-VB	Exp.	CINLIU ^{a,c}	HV-VB	Exp.	DULDIX ^{a,h}	HV-VB	Exp.	BENICL ^{a,i}	HV-VB	Exp.
C-Si-N	173.0	179.4	C-Si-C	133.6	118.8	O-I-C	85.0	78.6	Cl-I-Cl	171.1	179.1
C-Si-O	91.3	100.2	F _a -Si-F _a	174.1	172.5		84.9	79.6	C-I-Cl	94.5	92.2
	99.2	99.8	F _a -Si-F _e	93.0	86.3		169.9	158.2		94.5	87.1
	92.4	100.2		93.0	86.3						
N-Si-O	86.4	80.1	F _a -Si-C	88.8	92.0						
	87.8	79.6		88.8	91.9						
	86.3	80.1		88.8	91.8						
O-Si-O	104.7	117.5	C-Si-F _e	113.2	120.6						
	104.7	117.5		113.2	120.6						
	149.7	116.1									
 <p style="text-align: center;">3</p>			 <p style="text-align: center;">4</p>			 <p style="text-align: center;">9</p>			 <p style="text-align: center;">10</p>		
DALFOL ^{a,d}	HV-VB	Exp.	ADSBO ^{a,e}	HV-VB	Exp.	JAGCUP ^{a,j}	HV-VB	Exp.	IBZDAC ^{a,k}	HV-VB	Exp.
C-Si-O	103.4	106.7	C-P-O	102.6	108.1	O-I-O	92.9	81.1	O-I-O	174.9	163.1
	97.3	104.9		99.4	101.9		92.8	77.4	C-I-O	92.5	81.9
	99.7	106.6		99.4	107.8		174.4	158.0		92.5	81.2
	94.6	104.0		102.6	100.8						
O-Si-O	87.1	84.7	O-P-O	83.7	82.9						
	89.7	87.7		92.3	89.4						
	88.9	83.3		83.7	83.9						
	89.6	87.8		92.0	89.8						
	156.9	146.7		158.0	144.0						
	168.1	151.1		158.0	157.2						
 <p style="text-align: center;">5</p>			 <p style="text-align: center;">6</p>			 <p style="text-align: center;">11</p>			 <p style="text-align: center;">12</p>		
MSPBZP ^{a,f}	HV-VB	Exp.	MPLP ^{a,g}	HV-VB	Exp.	DUCCAF ^{a,l}	HV-VB	Exp.	PMeF ₄ ^m	HV-VB	Exp.
C-P-O	97.9	105.9	Cm-P-Ce	102.4	125.6	C-I-C	94.90	95.15	214	175.1	176.4
	98.1	102.3		156.2	123.4	O-I-C	85.95	73.88	213	89.3	NR ⁿ
	99.5	106.4		169.7	178.3		179.2	169.0	215	89.3	NR ⁿ
	99.2	101.4	Ce-P-Ce	102.4	111.0				216	94.2	91.8
O-P-O	84.7	83.0	Ca-P-Ca	169.7	178.3				413	88.1	NR ⁿ
	93.0	89.9	Cm-P-Ca	89.2	88.9				215	89.3	NR ⁿ
	84.0	89.5		90.6	89.8				415	88.1	NR ⁿ
	93.1	89.6	Ca-P-Ce	87.6	86.0				416	90.7	91.8
	162.6	147.7		88.4	95.6				316	121.0	122.2
	162.6	156.3		93.1	86.0				315	118.0	115.6
				97.0	94.0				516	121.0	122.2
 <p style="text-align: center;">13</p>			 <p style="text-align: center;">14</p>			 <p style="text-align: center;">15</p>					
						PMe ₂ F ₃ ^m	HV-VB	Exp.	PMe ₃ F ₂ ^m	HV-VB	Exp.
						416	174.2	179.8			
						412	91.0	NR ⁿ			
						413	91.8	NR ⁿ			
						415	87.1	89.9			
						612	91.0	NR ⁿ			
						613	91.8	NR ⁿ			
						615	87.1	89.9			
						213	122.5	124			
						215	119.2	118			
						315	118.3	118			

^a Cambridge Structural Database reference code. ^b Boer, F. P.; Turley, J. W.; Flynn, J. J. *J. Am. Chem. Soc.* **1968**, *90*, 5102. ^c Schomburg, D.; Krebs, R. *Inorg. Chem.* **1984**, *23*, 1378. ^d Holmes, R. R.; Day, R. O.; Chandrasekhar, V.; Harland, J. J.; Holmes, J. M. *Inorg. Chem.* **1985**, *24*, 2016. ^e Weiss, J.-V.; Schmutzler, R.; Chomburg, D.; Sheldrick, W. S. *Chem. Ber.* **1979**, *112*, 1464. ^f Wunderlich, H. *Acta Crystallogr., Sect. B.* **1974**, *30*, 939. ^g Day, R. O.; Husebye, S.; Holmes, R. R. *Inorg. Chem.* **1980**, *19*, 3616. ^h Nguyen, T. T.; Wilson, S. R.; Martin, J. C. *J. Am. Chem. Soc.* **1986**, *108*, 3803. ⁱ Archer, E. M.; van Schalkwyk, T. G. D. *Acta Crystallogr.* **1953**, *6*, 88. ^j Birchall, T.; Frampton, C. S.; Kapoor, P. *Inorg. Chem.* **1989**, *28*, 636. ^k Lee, C.-K.; Mak, T. C. W.; Li, W.-K.; Kirner, J. F. *Acta Crystallogr., Sect. B* **1977**, *33*, 1620. ^l Batchelor, R. J.; Birchall, T.; Sawyer, J. F. *Inorg. Chem.* **1986**, *25*, 1415. ^m Hellwege, K.-H. *Landolt-Boerstein Numerical Data and Functional Relationships in Science and Technology*; Springer Verlag: Berlin, 1976; Vol. 17. ⁿ Value not reported. ^o Culley, S. A.; Arduengo III, A. J. *J. Am. Chem. Soc.* **1984**, *106*, 1164.

bicyclo(3.3.0)octane (**7**) and diphenyliodonium-2-carboxylate (**11**) for which HV-VB computes the correct arrowhead distortion, but both are constrained to the arrowhead geometry by chelating groups.

Experimental trends²⁹ are reproduced by HV-VB computations for the series of mono-, di-, and trimethyl substituted fluorophosphines (**12**, **13**, and **14**, respectively). In each case the low energy site isomers are correctly predicted by HV-VB. That is, the methyl groups are substituted equatorially instead of axially. The axially substituted molecules are true minima but lie higher in energy than the site isomers with equatorial methyl groups. None of the equatorially substituted structures are ideal trigonal bipyramids, and HV-VB correctly computes the experimentally observed distortions. Fluorine is more electronegative than a methyl group, consequently fluorine prefers more p-character in its bonding orbitals. This leads to a trend of increasing bond angles in the series $F-P-F < F-P-Me < Me-P-Me$ for all three of the compounds which matches the trend found by experiment.

VII. The Role of Lone Pairs and the Relationship of HV-VB to the VSEPR Model

The structures of hypervalent main group complexes (*but not simple transition metal hydrides and alkyls*⁷¹) can be rationalized reliably with VSEPR theory. Primary tenets of the VSEPR theory⁶⁴ are (1) equilibrium geometries minimize repulsions between stereochemically active electron pair domains, (2) bond pairs occupy less volume than lone pairs, and (3) the domain of a bond pair decreases in volume as the electronegativity of the ligand increases. Each of these tenets has a corresponding valence bond rule: (1) equilibrium geometries minimize non-orthogonalities of hybrid orbitals, (2) lone pairs prefer high s-character yielding a large, bulbous shape, and (3) more electronegative ligands prefer higher p-character in the bond forming hybrids.

The significant areas of difference between VSEPR and qualitative valence bond theory concern matters of emphasis. In valence bond theory, the directionality of bond pairs originates in the use of available valency to make electron pair bonds with optimal concentration of electron density in the internuclear region. The structures of simple transition metal hydrides highlight these differences with particular clarity. We have shown previously⁷¹ that the C_{3v} global minimum structure for WH_6 and MoH_6 as well as the existence of C_{3v} and C_{5v} local minima can be understood as a natural stereochemical consequence of sd^5 hybridization of the metal atom. Although VSEPR theory generally is not used to rationalize the geometries of metal complexes, application of the principle VSEPR tenets to six equivalent bond pairs of WH_6 necessarily predicts minimal interbond repulsions at the octahedral geometry. Based on computations, the octahedral geometry is predicted to be approximately 140 kcal/mol higher in energy than the C_{3v} geometry.⁷² Thus it would appear that the qualitative ideas of valence bond theory, as represented in the VALBOND and HV-VB schemes, lead to a more general understanding of the forces controlling molecular geometries.

For hypervalent main group compounds, such as ClF_3 , the VSEPR and the HV-VB schemes both predict the T-shaped geometry, but the emphases are different. In HV-VB emphasis is placed on the preference of $3c-4e^-$ bonding elements for linear arrangement and the high p-character of Cl-F covalent

bonds. Indeed, the consideration of lone pairs is not required to arrive at the T-shape. In contrast, VSEPR theory begins with an approximate equivalence of stereochemical activity for all electron pairs around the central atom to arrive at a trigonal bipyramidal arrangement of electron pairs. Further refinement of the volumes of different electron pair domains yields a preference of the lone pairs for the equatorial positions. Significantly, these considerations allow VSEPR theory to rationalize the small distortions to the arrowhead geometry.

Although the VALBOND scheme de-emphasizes the stereochemical role of lone pairs, it seems that the model might be improved by the inclusion of explicit lone pairs. In principle, one should be as concerned with nonorthogonalities involving lone pair hybrid orbitals as with those of bond hybrid orbitals.⁷³ Pragmatically, their inclusion may improve modeling of the distortion of, e.g., ClF_3 away from the idealized T-shape. Therefore we have performed a set of computations to explore the consequences of explicit lone pairs in the force field. For ClF_3 we generate equivalent lone pairs and assign to them hybridizations of sp^1 . This hybridization is derived as follows: the primary resonance structures involve a ClF_2^+ fragment and a fluoride anion. Assuming that the Cl-F bonds of the ClF_2^+ fragment prefer high p-character, one s and one p orbital are available to lone pairs, hence, sp^1 hybridization. We assume that lone pairs are ineffective in stabilizing $3c-4e^-$ bonding interactions and assign them electronegativities of 0. Finally, the HV-VB parameter for lone pairs is set to 125 kcal/mol, or 1/2 of the default value, because we assume that lone pairs should be more readily deformed due to the absence of strong attraction to a second nucleus. With this reasonable, albeit somewhat arbitrary, model we find that the geometrical features of ClF_3 are brought into closer accord with experiment ($\angle F_{ax}-Cl-F_{ax}$: 178° vs 177° (exp); $\angle F_{ax}-Cl-F_e$: 87° vs 88° (exp)). Thus, explicit lone pairs can lead to a better MM description of potential energy surfaces. Another example for which the explicit inclusion of lone pairs is likely to aid the reproduction of experimental structures is the case of XeF_6 . One of the early successes of VSEPR theory was the prediction of a nonoctahedral structure for XeF_6 . We anticipate that the explicit inclusion of a lone pair with even a small amount of p-character will result in a slight distortion of XeF_6 from the octahedral shape. A lone pair of pure s-character would not effect such a distortion due to the spherical nature of the s-orbital.

There are drawbacks to the inclusion of explicit lone pairs in the VALBOND and HV-VB; primarily these drawbacks concern increased computation times, reparametrizations, the possibility of major perturbations of computed amine and phosphine inversion barriers, etc. Furthermore, refinements in the treatment of 1,3 van der Waals and electrostatic interactions also should be considered in improving the description of molecular shapes. An effort to include 1,3 van der Waals and 1,3 and 1,2 electrostatics is underway by introducing the HV-VB method into the UFF force field of Rappé and co-workers.¹⁵ These results will be reported in future publications.

VIII. Summary

In their common implementation, MM computations are essentially a ball-and-spring mechanical model of molecular structures and energies. These computations are largely empirical; one could view these common MM methods as functions that interpolate between extremes of many pieces of empirical data. We have shown that a connection between MM computa-

(71) Landis, C. R.; Cleveland, T.; Firman, T. K. *J. Am. Chem. Soc.* **1995**, *117*, 1859–1860.

(72) Shen, M.; Schaefer, H. F.; Partridge, H. *J. Chem. Phys.* **1992**, *98*, 508.

(73) Pauling, L. *The Nature of the Chemical Bond*; Cornell University: Ithaca, 1960.

tions and more fundamental bonding theories can be effected by basing the derivation of MM potential energy functions on the principles of valence bond theory. As first noted by Maksic over two decades ago,^{74,75} the concept of hybridization is particularly useful in forging this connection. In this paper we have shown that the inclusion of another valence bond concept, resonance, improves the MM description of hypervalent molecular shapes. The influence of resonance is modeled through (1) the description of hypervalent molecules as a weighted composite of different MM configurations and (2) a special potential for the angular dependence of $3c-4e^-$ bonding interactions. Different MM configurations are generated by scanning all possible arrangements of $2c-2e^-$ and $3c-4e^-$ bonding interactions. The weighting coefficients for these configurations are geometry dependent. For nonhomoleptic hypervalent molecules, the relative energies of different MM configurations are offset according to the electronegativities of the ligands involved in $3c-4e^-$ bonds. The potential energy function for the $3c-4e^-$ interactions is modeled as a donor-acceptor interaction involving donation of a lone pair from the ligand into a σ^* orbital.

The effect of incorporating valence bond concepts into the HV-VB scheme is a more authentic representation of the potential energy surfaces for hypervalent main group complexes. Thus we find that equilibrium geometries are modeled well, vibrational frequencies are reproduced with acceptable accuracy, the site preferences of different ligands for engagement in $3c-4e^-$ bonds are accommodated, the fluxional pathways of hypervalent molecules are predicted with close correspondence to those predicted by *ab initio* methods, and the hypervalent

(74) Kovacevic, K.; Maksic, Z. B. *J. Org. Chem.* **1974**, *39*, 539.

molecules are free to undergo ligand site exchange during dynamics simulations. To the best of our knowledge, no previous MM methods have been able to address these issues so robustly. The HV-VB scheme is quite general: T-shaped, seesaw, trigonal bipyramidal, and octahedral hypervalent molecules share a common scheme and only generic, rule-based parameters are used. Furthermore, none of the concepts used in the HV-VB scheme conflict with localized bond descriptions of high quality electronic structure computations. For example, correct hypervalent geometries are computed without resorting to d-hybridization about the central atom.

The ideas embodied in the HV-VB method apply to transition metal complexes, also.⁷¹ For example, the preference of PtH_4^{2-} for a square planar geometry can be understood as the consequence of an electronic structure comprising two $3c-4e^-$ bonds and four lone pairs. The application of these concepts to transition metal complexes is the topic of a forthcoming publication.

Acknowledgment. This work was supported by a grant from the National Science Foundation (NSF-CHE9112988). We gratefully acknowledge Professor Frank Weinhold's assistance with the NBO program.

Supporting Information Available: Table of HV-VB parameters used in the computations and selected *ab initio* data (3 pages). Ordering information is given on any current masthead page.

JA9506521

(75) *Directional Properties of Covalent Bonds in Molecules*; Maksic, Z. B., Ed.; Springer-Verlag: Berlin, 1990; Vol. 2.